Iranian Journal of Chemical Engineering
Vol. 17, No. 1 (2020), IAChE

CFD Modeling of Hydrocarbon-Air System Hydrodynamics in Three Types of Column Reactors

H. Faraji [1], ***A. Habibi*** [1*], ***E. Jalilnejad*** [2]

[1] *Faculty of Petroleum and Chemical Engineering, Razi University, Kermanshah, Iran*
[2] *Faculty of Chemical Engineering, Urmia University of Technology, Urmia, Iran*

ARTICLE INFO

Article history:
Received: 2020-04-14
Accepted: 2020-08-17

Keywords:
Hydrodynamics
Multiphase Reactor
Gas Flow Velocity
Mass Transfer Coefficient
Gas Holdup
Dead Zones
Net Draft Tube

ABSTRACT

In this study, hydrodynamic characteristics such as the gas holdup (ε), the liquid phase velocity, and the mass transfer coefficient (k_La) for an air-diesel system were modeled for the bubble column (BCR), the airlift (ALR), and the airlift with the net draft tube (ALR-NDT) reactors at different superficial gas velocities ranging from 0.008 to 0.085 m s^{-1}. A 3D two-fluid Eulerian-Eulerian model was developed using the computational fluid dynamic (CFD) technique to model the three configurations of column reactors and predict the hydrodynamic parameters. The results of the 3D-CFD modeling showed good agreement with the experimental data where the average error was less than 14 and 9 % for ε and k_La respectively. Although the vortex occurred in BCR and ALR at high gas velocities, the optimum liquid and the gas circulation and distribution were observed in ALR-NDT. Furthermore, the formation of the dead zone (k_La = 0) in the reactors was studied, and the results revealed that ALR-NDT has a lower volume of dead zones (about 8 %) in comparison with BCR and ALR. In order to reduce the dead zone in BCR and ALR systems, the location of the gas diffuser and the draft tube was investigated. The dead zone was decreased by 12 % with shifting the gas diffuser to the bottom of the BCR. Also, by increasing the distance of the gas diffuser from the draft tube, the dead zone was decreased by 40 % specifically near the walls of ALR. Meanwhile, the simultaneous shifting of the gas diffuser and the draft tube to a lower position in ALR had no effect on the dead zone formation and its distribution.

1. Introduction

The multiphase contactors are extensively used in the biochemical fermentation, the biological wastewater treatment and chemical, petrochemical, and metallurgical industries. Among the multiphase contactors, the bubble column reactor (BCR) and the airlift reactor (ALR) as the air agitating systems, have an industrial importance due to the simplicity of design, lower operating and preservation costs, the high heat and mass transfer performance, and the absence of movable segments [1, 2]. In both reactors, the continuous phase is liquid while air is dispersed in the form of bubbles by a diffuser at the bottom of the reactor vessel which

[*]Corresponding author: a.habibi@razi.ac.ir

provides the circulation and mixing of the phases. The driving force for the liquid circulation is improved by the gas holdup (ε_g) difference between riser and downcomer sections in the ALR design.

Extensive studies were performed to understand the relationships between the operational factors such as the superficial gas velocity (u_g) and hydrodynamic characteristics i.e., the gas holdup and the volumetric mass transfer coefficient (k_La) in BCR and ALR systems [3]. The size and velocity distribution of bubbles has a significant role in the control of hydrodynamic features in the reactors. The hydrodynamic of the reactors also depends on the column interior design (i.e., diameter and height) and the bubble diffuser design. Fu et al. [4] studied the performance of ALR-NDT for the alcoholic fermentation of glucose using biomass and revealed that ALR-NDT works with a higher performance in comparison with BCRs and ALRs in terms of the mixing efficiency, the oxygen transfer, and productivity. However, most of the studies on ALR-NDT have been limited to the aqueous systems, and few experimental data are available for oil-based fluids, while the study of the petroleum-based liquids like diesel is crucial for development of bio-desulfurization processes [5].

Since the determination of hydrodynamics in air-agitating tanks is extremely complex, the computational fluid dynamic (CFD) modeling provides a tool for understanding more details of these systems [6]. Generally, Euler-Euler and Euler-Lagrange methods are two fundamental approaches which could be used to simulate the flow dynamics of two-phase gas-liquid systems. Euler-Euler method is a fundamental macroscopic model of the two-phase fluid flow approach in which both the liquid and the gas phase movements are contemplated as homogeneous or interpenetrating continua [7, 8]. The Euler-Lagrange method represents only the continuous phase through the Navier-Stokes equations. The simulation of water-air system in an ALR with the Euler-Euler solving method was previously conducted and the optimum distance of the draft tube from the wall was determined to achieve an effective mixing, higher rotary movements of the gas and liquid phases, and improve the reactor performance [9]. Also, the hydrodynamics of a laboratory scale ALR with an internal loop was studied using Euler-Lagrange model at three different geometries using COMSOL Multiphysics software [8]. Their results showed an error of ± 10 % for the gas holdup and the liquid circulation velocity for low inlet gas volumetric flows for medium and large size draft tubes, while the results for a high inlet volumetric flow and smaller draft tube had a noticeable error. Nalband and Jalilnejad (2019) simulated the gas holdup in ALR-NDT as an important hydrodynamic parameter in the air-water system using a two-phase flow model provided by the bubbly flow application mode [10]. They used the drag model of “Large Bubble” in the CFD simulation that was introduced by Sokolichin et al. to obtain the gas holdup and k_La distribution along the reactor as well. Lu et al. (2019) investigated the effect of the superficial gas velocity on the flow structure with the 3D CFD simulation of an external loop airlift reactor for a water-air system and compared results with the bubble plume and the velocity field of the riser that were captured using the particle image velocimetry technique. The results showed that the gas-liquid two-phase flow in the riser was always unsteady and also the gas holdup increased

with the increase of the superficial gas velocity, while the liquid axial velocity showed a trend of first increasing and then decreasing [11]. Guler et al. (2020) used CFD to simulate and investigate the flow patterns and the profile of gas holdup within 2L photo-bioreactor. The gas holdup as a hydrodynamic characteristic of the photo-bioreactor, showed a difference between the riser and the downcomer regions. Also, velocity profiles of the fluids inside the draft tube were higher than that of obtained in the downcomer region. However the liquid circulation was achieved from the draft tube to the downcomer region and mixing was not provided effectively considering the turbulence kinetic energy [12].

The aim of the present study is to develop a 3D transient CFD model for the simulation of hydrodynamic behaviors of the air-diesel system at different superficial air velocities ranging from 0.008 to 0.085 m s^{-1} in BCR, ALR, and ALR-NDT. It is worth mentioning that the CFD modeling of the hydrodynamic parameters for the diesel-air system in three different configurations of bubble columns has not been reported and compared in the literature specifically for ALR-NDT as a modified type of conventional ALRs. The validation of the simulations were determined by comparing the simulation results with experimental data obtained previously at our laboratory [13]. The effects of superficial air velocities on the hydrodynamics and mass transfer coefficient were discussed. Also, the dead zones (where the k_La was equal to zero) were determined and compared for the three types of reactors.

2. CFD modeling

2.1. Experimental setup

The schematic view of the experimental apparatus and also the geometric specifications of the reactors can be seen in Fig. 1. The working volume of the test reactor was 2.1 L, and air was sparged into the reactor through a gas diffuser (the diameter of 5 cm and the hole size of 100-160 μm) placed at the height of 5 cm above the bottom of the reactor. The reactor without and with the use of a solid draft tube was considered as BCR and ALR respectively. ALR-NDT was made by the replacement of the solid draft tube with a cylindrical shape stainless steel tube with a mesh size of 12. A calibrated rotameter was used for controlling the aeration rate in the reactors and temperature in all experiments was fixed at 25 ^oC using a thermostat circulation tank. The systems were at atmospheric pressure condition, and the air aeration system provided the driving force for the circulation of liquid phase (diesel) in the reactors. The superficial air velocity ranged from 0.008 to 0.085 m s^{-1}. The physicochemical specifications of the diesel and air used in this study are summarized in Table 1.

2.2. Mathematical modeling

The two-fluid model for the bubbly flow is commonly used for modeling bubble column reactors which could easily develop a multiphase flow model for gas bubbles rising through a liquid [2].

Table 1
Properties of the fluid phases used in the CFD simulation.

Fluids	ρ (kg m^{-3})	ν ($\times10^{-6}$ m^2 s^{-1})	σ (mN m^{-1})	D_{O2} ($\times10^{-9}$ m^2 s^{-1})
Diesel	815.23	3.46	25.6	1.66
Air	1.225	14.8	-	-

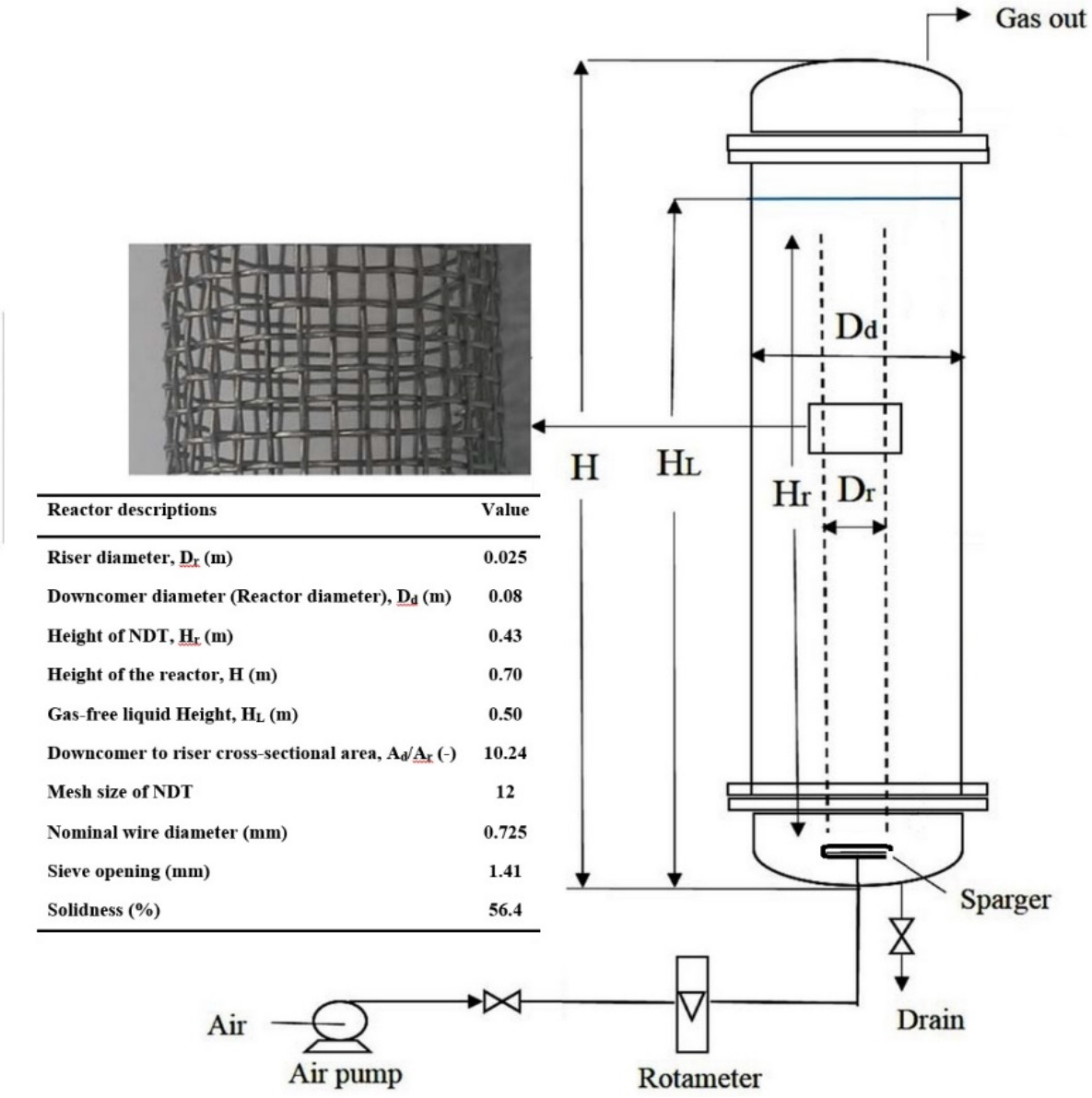

Reactor descriptions	Value
Riser diameter, D_r (m)	0.025
Downcomer diameter (Reactor diameter), D_d (m)	0.08
Height of NDT, H_r (m)	0.43
Height of the reactor, H (m)	0.70
Gas-free liquid Height, H_L (m)	0.50
Downcomer to riser cross-sectional area, A_d/A_r (-)	10.24
Mesh size of NDT	12
Nominal wire diameter (mm)	0.725
Sieve opening (mm)	1.41
Solidness (%)	56.4

Figure 1. Schematic view and geometric specifications of the reactors used at the 3D-CFD simulation.

Thus, a two-fluid Eulerian-Eulerian model has been adopted to simulate the test reactors in this study and mass transfer coefficient, volume fraction of the gas phase (gas holdup) and dead zones have been obtained based on the developed bubbly flow model [14, 15]. Tracking the averaged concentration of the phases has been conducted by treating the two phases as interpenetrating media in this model. A momentum balance equation and a continuity equation describe the dynamics of each phase. The momentum equation for the liquid phase can be written as:

$$\varphi_l\rho_l\frac{\partial u_l}{\partial t}+\varphi_l\rho_l(u_l\cdot\nabla)u_l=\nabla\cdot\left[-p_l+\varphi_l\mu_l\left(\nabla u_l+(\nabla u_l)^T\right)\right]+\varphi_l\rho_l g+F \quad (1)$$

where the continuity equation is:

$$\frac{\partial}{\partial x}\left(\rho_l\varphi_l+\rho_g\varphi_g\right)+\nabla\cdot\left(\rho_l\varphi_l u_l+\rho_g\varphi_g u_g\right)=0 \quad (2)$$

where u is the velocity vector (m s^{-1}), ρ is the density (kg m^{-3}), φ is the phase volume fraction (m^3 m^{-3}), p is pressure (Pa), g is the gravity vector (m s^{-2}), F is any additional volume force (N m^{-2}), and μ is viscosity (Pa.s). The subscript "l" and "g" denotes quantities relevant to the liquid phase and the gas phase respectively.

The gas phase transport equation is:

$$\frac{\partial y}{\partial x} + \nabla \cdot \left(\rho_g \varphi_g u_g\right) = -m_{gl} \tag{3}$$

where m_{gl} is the mass transfer rate from the gas to the liquid (kg m^{-3} s^{-1}).

The liquid volume fraction is calculated from [16]:

$$\varphi_l = 1 - \varphi_g \tag{4}$$

and the gas velocity is determined by:

$$u_g = u_l + u_{slip} \tag{5}$$

where u_{slip} is the relative velocity between the gas and the liquid.

The gas holdup could be experimentally measured by the following expression:

$$\varepsilon_G = \frac{V_f - V_i}{V_f} = \frac{h_f - h_i}{h_f} \tag{6}$$

where V_f and V_i are the volumes of the aerated and un-aerated liquid respectively, and h_f and h_i are aerated and un-aerated liquid heights, respectively.

In a low gas volume fraction ($\varphi_g \sim 0.01$), the momentum and continuity equations can be rewritten as follows:

$$\begin{aligned}\varphi_l \rho_l \frac{\partial u_l}{\partial x} + \varphi_l \rho_l u_l \cdot \nabla u_l \\ = -\nabla_p + \nabla \\ \cdot \left[\varphi_l (u_l + \mu_T)\left(\nabla u_l + \nabla u_l^T\right)\right] \\ + \varphi_l \rho_l g + F\end{aligned} \tag{7}$$

$$\rho_l \nabla \cdot u_l = 0 \tag{8}$$

For bubbles rising through the liquid, due to buoyancy, it is proper to presume that the pressure forces approximately balance the viscous drag forces on the gas bubbles as follows:

$$-\nabla p = C_d \frac{3}{4} \frac{\rho_l}{d_b} |u_{slip}| u_{slip} \tag{9}$$

where d_b is bubble diameter, and C_d (dimensionless) is the viscous drag coefficient.

Since the bubble diameter is assumed to be 130 μm (< 2 mm) in the present study, thus, Hadamard–Rybczynski model is used for predicting drag coefficient, which is defined as [17, 18]:

$$C_d = \frac{16}{Re_b} \tag{10}$$

$$Re_b = \frac{d_b \rho_l |u_{slip}|}{\mu_l} \tag{11}$$

Accurate simulation of a reactor system mainly depends on the application of proper turbulence models by CFD which can precisely characterize the present flow fields. Among a large family of turbulence closures (zero-, one-, and two-equation, etc.), the standard k-ε turbulence model is the most commonly used for modeling medium to large scale applications as it is a tradeoff between the computational accuracy and efficiency and is based on the eddy viscosity concept. A zero shear stress condition and an outlet for the dispersed phase (the gas phase) are considered in this model, thus, a symmetric plane is assumed for the free surface in the liquid phase. The standard k–ε model is essentially a high Reynolds number model and assumes the existence of isotropic turbulence and the spectral equilibrium [19, 20]. It is less expensive than more advanced models such as the RSM model and performs

quite well for boundary layer flows. Thus, the k-ε turbulence model was used and solved in the present work. The k-ε model solves two extra transport equations for two additional variables. The first one is the turbulent kinetic energy (k), and the other one is the dissipation rate of turbulent energy (ε). The turbulent viscosity is modeled with [21]:

$$\mu_T = \rho_l C_\mu \frac{k^2}{\varepsilon} \tag{12}$$

where C_μ is a model constant. The values of k and ε as the turbulent kinetic energy and the dissipation rate of turbulent energy are calculated by the following closure equations [8, 10, 15]:

$$\rho_l \frac{\partial k}{\partial t} + \rho_l u_l \cdot \nabla k = \nabla \cdot \left[\left(\mu_l + \frac{\mu_T}{\sigma_k}\right)\right] + P_k - \rho_l \varepsilon + S_k \tag{13}$$

$$\rho_l \frac{\partial \varepsilon}{\partial t} + \rho_l u_l \cdot \nabla \varepsilon = \nabla \cdot \left[\left(\mu_l + \frac{\mu_T}{\sigma_\varepsilon}\right)\nabla \varepsilon\right] + C_{\varepsilon l}\frac{\varepsilon}{k} C_{\varepsilon l} P_k - \rho_l C_{\varepsilon l}\frac{\varepsilon^2}{k} + C_\varepsilon S_k \frac{\varepsilon}{k} \tag{14}$$

The values of the constant parameters used in the k-ε model are [21]:

$$C_\mu = 0.09\,, C_{\varepsilon l} = 1.44\,, C_{\varepsilon 2} = 1.92\,, \sigma_k = 1\,, \sigma_\varepsilon = 1.3 \tag{15}$$

The volumetric mass transfer coefficient (k_La) is of great importance in gas-liquid systems. Various empirical equations have been introduced to calculate the gas-liquid mass transfer in bubbly flows. These empirical equations are based on empirical data that are limited to a specific range relating their variables to theoretical equations based on the renewal theory, the penetration theory, the two-film theory or the combination of penetration and two films theories. For modeling mass transfer coefficient, Cockx et al. [22] suggested a contact time based model which was based on the penetration theory of Higbie for local mass transfer assessment. According to that theory, a new interfacial surface was created at its further point, when gas bubbles were moving through the liquid. A non-stationary diffusion was attained from the liquid phase to the gas-liquid interface during the contact exposure time [23]. The suggested equation by Cockx et al. is [22]:

$$k_La = \frac{12\varepsilon_G}{d_b}\sqrt{\frac{D_L u_{slip}}{\pi d_b}} \tag{16}$$

where D_L is the molecular diffusivity of the gas in the liquid.

The specific interfacial area (a) can be estimated based on the predicted local gas holdup value by the following equation:

$$a = \frac{6\varepsilon_G}{d_b} \tag{17}$$

2.3. Boundary conditions

In this study, the entire volume of the three reactors, including the draft tube was considered as the isothermal (298 K) computational domain and the symmetrical boundary condition was applied along the vertical centerline of the computational domain. Regarding the aeration rate applied to the reactors, "laminar bubbly flow" and "turbulent bubbly flow" physical interfaces were used. The sparger was placed 5 cm above the bottom of the reactor and the gas flux condition was used for the net draft tube input. The boundary conditions for the top of the reactors were defined as the gas outlet and the slip condition for gas and liquid phases respectively. The outlet pressure of the top free surface of the reactor was assumed to be the atmospheric pressure and the gas could

freely leave the surface. For the walls of the internal reactors, the "no slip" (the wall function) was used as boundary condition for the liquid phase, while the "No gas flux" condition was used for the gas phase.

The developed CFD model is based on the following assumptions: (a) the gas density is negligible compared with the liquid density; (b) the balance between the viscous drag and pressure forces is responsible for the motion of the gas bubbles relative to the liquid; (c) the two phases share the same pressure field; (d) the gas and liquid phases are not chemically reacting; (e) the interaction between bubbles is ignored; (f) the inlet bubble diameter is assumed to be constant (130 μm) in this work.

2.4. Geometry and meshing

For ALR, an internal draft tube was located at 0.06 m above the bottom of the reactor with the radius equal to that of the diffuser (0.025 m). Also in the case of ALR-NDT, a net draft tube with a mesh size of 12 and a height of 0.43 m was located at 0.06 m above the bottom of the reactor. The unstructured meshing was applied to the computational domain, and 3D computational grid was generated as shown in Fig. 2 for the three configurations of reactors. CFD models were solved numerically on meshes discretized in a 3D computational domain. The quality of the mesh played an important role in the accuracy and stability of the numerical computation. The discretization error would vanish only if the grid spacing tended toward zero. A proper number of meshes should be determined as a compromise between the computation efficiency and accuracy [23]. Thus, a mesh independency test was performed to the three configurations of the tested reactors as the first verification step of the CFD calculations. The reactors used in that work were divided into smaller cells by free triangular and tetrahedral unstructured meshes. In a simple mesh independence test, three mesh systems were used for checking the independency of the grid and selecting an optimized number of grids. Table 2 displays the influence of the number of meshes on the gas holdup value at a fixed gas velocity (Ug= 0.041 m s-1). The gas holdup difference between cases 2 and 3 was negligible for all the test reactors and thus, case 2 was selected for simulation of the reactors to save computational time and energy.

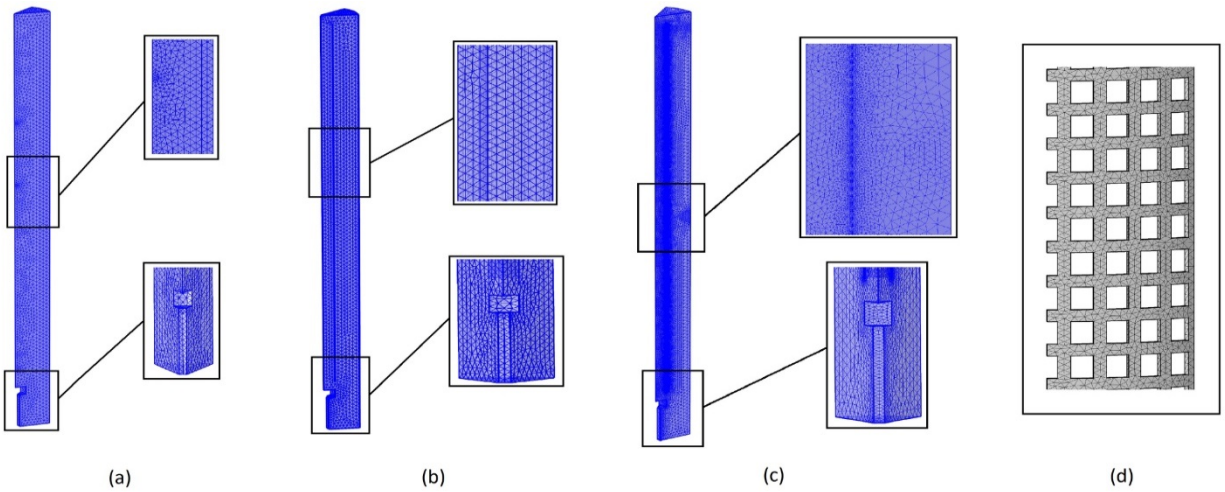

Figure 2. The symmetric 3D geometry with the unstructured refined mesh generation of BCR (a), ALR (b), ARL-NDT (c), and the net draft tube mesh distribution (d).

Table 2
Mesh independency check.

Reactor type	Number of case	Number of cells	Gas holdup
BCR	1	25792	0.0171
	2	61106	0.0197
	3	222218	0.0203
ALR	1	28508	0.0159
	2	63741	0.0175
	3	218752	0.0180
ALR-NDT	1	626525	0.0109
	2	1829396	0.0129
	3	2425930	0.0136

2.5. Numerical solution

Simulation processes of the reactors were carried out using COMSOL Multiphysics (version 5.2). For the geometrical design, due to the symmetry of the reactor configurations, the vertical one-eighth section of the reactors was modeled to reduce the run time. A time-dependent segregated solver was used for the calculation and the convergence was satisfactory at the criteria 10^{-4}. The time step for unsteady-state equations was considered as 10-3 s. The computation of simulation was carried out on a cloud computing system with Intel Xeon 10core and 16GB RAM and the maximum computing time to obtain the results was 42 min which was for ALR-NDT.

3. Results and discussion

3.1. Validation of simulation

The gas holdup is among important hydrodynamic parameters in air agitating vessels. The temporal change of the gas holdup in the test systems is presented at Fig. 3. The results show that the steady-state is achieved in the systems after 30 seconds where the average of the gas holdup becomes stable for different superficial gas velocities. At BCR, as shown in Fig. 3, the absence of any draft tube which segregates the inlet flow results in air bubbles coalescence and makes large bubbles. The inhomogeneity of air bubbles and the absence of a regular circulation cause the reduction of the gas holdup in BCR. However, the air entrapment inside of the draft tube leads in a higher average gas holdup for ALR in comparison with BCR. The air entrapment in ALR continues until the height of the gas phase reaches the surface of the gas-free liquid and the excessive air exits from the gas outlet and the rest circulates and enters the downcomer region. This phenomena results in a slope reduction at that point in the graphs. The break-point is significantly observed in ALR-NDT due to the netted structure of the draft tube that increases the possibility of the air entrapment in the net draft tube between netted wires.

In this study, the steady state values of the gas holdup are compared with experimental data at different superficial gas velocities in the test systems as shown in Fig. 4. The variation of the gas holdup has been from 0.005 to 0.027 when aeration rate was increased from 0.008 to 0.085 m s^{-1} in BCR respectively and the 3D-CFD simulation was predicted this behavior with a total error less than 5.8 % as seen in Fig. 4a. The comparison of the results of Fig. 4 indicated that the difference between experimental data and simulation values was higher for ALR and ALR-NDT. However, the difference was

decreased by the increase of the aeration rate in the systems. The error between the experimental and simulation data could arise from several sources such as the initial assumptions that were made, numerical solutions, incomplete iterations and other calculation parameters. Another reason for the poor CFD prediction could be related to the uncertainty in the experimental measurement of the hydrodynamic parameters in the test reactors due to their small size which was also stated by Chisti (1998) [24]. The inaccuracy of experimental results are due to limitations of measuring devices and human errors especially in small column reactors. Similar trends were reported in different researches i.e. increasing of gas holdup was reported in the literature by increasing gas flow rate from 0.01 to 0.04 m s^{-1} when the turbulent model was used for a BCR for the biodiesel production [25]. In ALRs, with the increment of superficial gas velocity, the gas-phase displacement increases and it concludes to a fast transfer of the gas phase to the top and the release of the air form the top surface. So, the increase of the superficial gas velocity decreased the gas holdup in ALRs [26]. Similar results were also notified by Lu et al. and the increasing relationship between the velocity profile and the gas holdup was reported in their research [11]. On the basis of the previous findings, in the test reactors the superficial gas velocity ranging 0.008- 0.020 m s^{-1} corresponded to the laminar flow while the turbulent regime was only obtained at a superficial gas velocity of 0.032-0.085 m s^{-1} [13]. It is worth mentioning that the gas holdup in BCR was more affected by the aeration rate when compared with ALR and ALR-NDT systems as it is clear at Fig. 4. Also, ALR-NDT and BCR performance on the gas holdup was better than ALR, and it is in agreement with previous reports in aquatic systems [27]. However, the higher viscosity of diesel in comparison to water makes this liquid to gain lower gas holdup values than water at the same aeration rate when compared to the air-water system [10]. In fact, the petroleum-based liquid systems due to the decrement of surface tension have less bubble breakage characteristic than water [28].

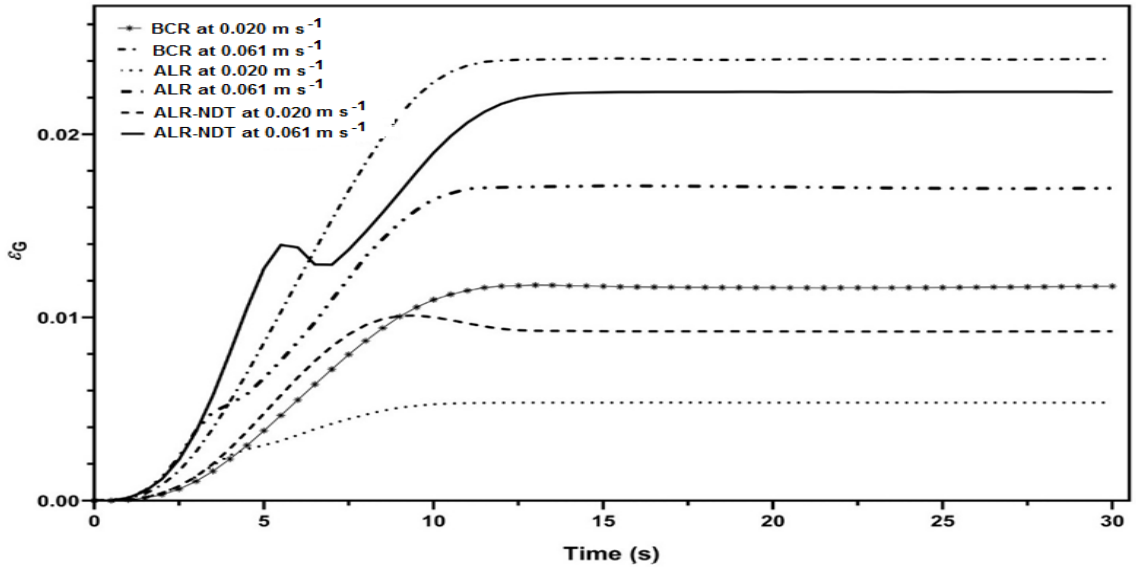

Figure 3. Time dependency of the gas holdup for the diesel-air system at BCR, ALR, and ALR-NDT when the aeration rate was set on 0.020 m s^{-1} (laminar regime) and 0.061 m s^{-1} (turbulent regime).

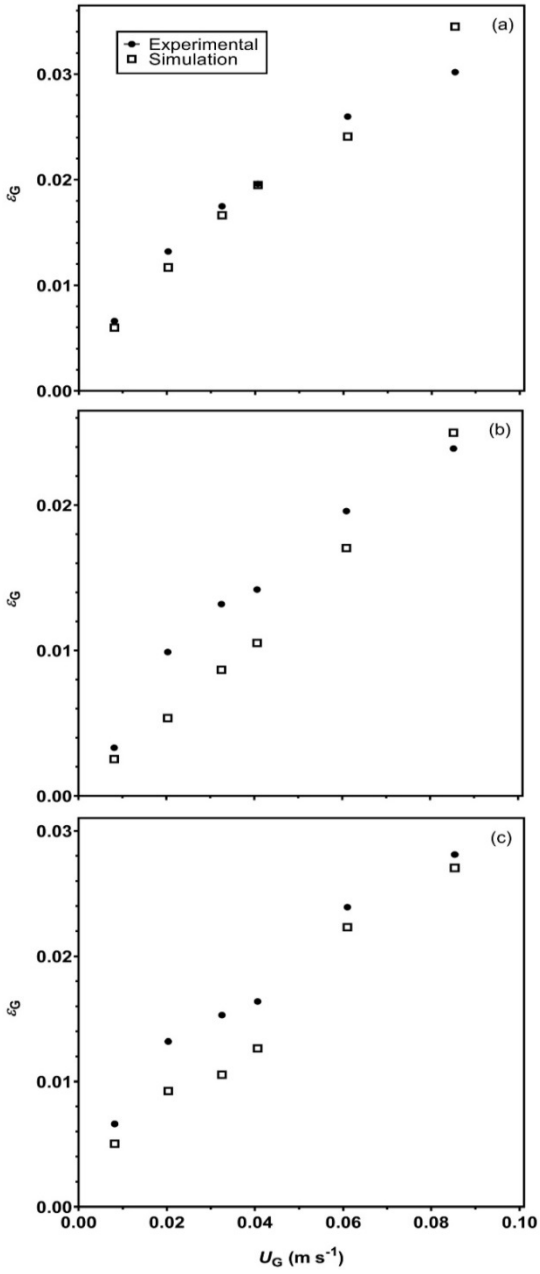

Figure 4. Comparison of the experimentally measured gas holdup and the values predicted by the 3D-CFD simulation as a function of the superficial gas velocity at BCR (a), ALR (b), and ALR-NDT (c).

3.2. Mass transfer coefficient

The volumetric mass transfer coefficient (k_La) is one of the most important transport characteristics used in the scale-up, design and performance optimization of mechanically agitated gas-liquid contactors. The k_La value as the function of U_G is presented at Fig. 5. It can be seen at Fig. 5a that k_La is increased by increasing the gas velocity from 0.008-0.020 m s^{-1} (the homogeneous flow regime). The bubble flow pattern in BCR is non-uniform and due to the incidence of the vortex and non-uniform recirculation of bubbles, the growth rate of mass transfer coefficient decreases in BCR and a slight increase is seen in the k_La value. It should be mentioned that the maximum error for BCR was 3.88 %. When it comes to ALR as shown at Fig. 5b, due to the presence of the draft tube inside of these vessels, the phase circulation and distribution are affected resulting in lower k_La values for the system in comparison to BCR. The k_La value was significantly increased at ALR for $U_G \geq 0.061$ m s^{-1}, mainly due to the gas circulation specifically in the downcomer section. In a similar research, Tunthikul et al. reported that by achieving an optimized configuration for A_d/A_r, nevertheless, the increase of the gas flow velocity would increase the gas-liquid interfacial area, and hence, directly effecting the proliferation of the volumetric mass transfer coefficient [29]. The total error value for the estimation of the ALR behavior was 10.76 %. Also, the k_La value was determined for NDT-ALR system as presented at Fig. 5c where the effect of NDT on the bubble breakup and the increase of the gas-liquid interfacial area, resulted in higher k_La values of ALR-NDT in comparison to the conventional ALR. In the research done by Nalband and Jalilnejad the same results and trends were reported for the effect of the superficial gas velocity and the presence of the net draft tube on the increasing trend for the volumetric mass transfer coefficient in the air-water system [10]. As shown at Fig. 4 and 5, the developed CFD model resulted in an underestimation in simulation results

compared to the experimental data. Beside the error sources mentioned in the previous section, the bubble diameter has a significant effect on the gas holdup and the mass transfer coefficient of column reactors. Thus, the assumed bubble diameter seems to be the main source of the difference between the experimental and simulation results. Therefore, it is necessary to consider the variations of the bubble diameter using bubble distribution methods which are not considered in this work and surely are the main source of error in this study. The modeling errors in experiments and numerical simulations are epistemic and due to ignoring physical problems, so, there are different solutions that could reduce these errors. It could be concluded that, in spite of some deviations, CFD could generally predict the real behavior of the reactors with an acceptable accuracy.

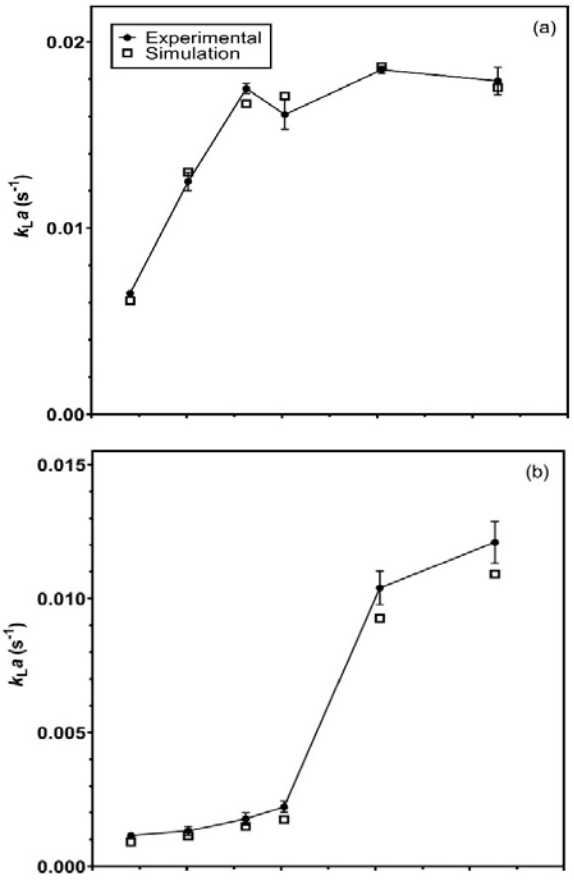

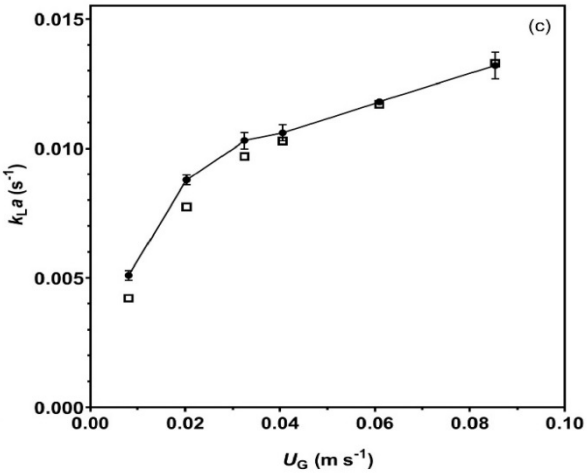

Figure 5. Comparison of the experimentally measured mass transfer coefficient and the values predicted by 3D-CFD simulation as a function of the superficial gas velocity at BCR (a), ALR (b), and ALR-NDT (c).

3.3. Flow modeling of BCR, ALR, ALR-NDT

It is clear that diesel as a liquid phase is different from water in terms of viscosity, density and the surface tension, and thus it is expected that the gas dispersion and the liquid circulation are changed in the diesel-air system. Fig. 6 shows the liquid flow patterns in the test reactors. The results at Fig. 6a obviously shows the formation of vortex at above the gas diffuser in BCR. However, the vortex did not have sufficient power for mixing the gas phase into the liquid phase at Ug < 0.061 m s^{-1} (the gas volume fraction was lower than 0.02). With increasing the gas inlet velocity up to 0.085 m s^{-1}, the formation of the strong vortexes improved the mixing behavior in the system and the gas volume fraction in diesel was increased to about 0.08. Fig. 6b shows the effect of the insert tube on the mixing behavior of ALR. The insert tube modified the circulation pattern of the liquid phase in the reactor and prevented the accumulation of vortexes near the gas diffuser. The difference of the gas volume

fraction between the riser and downcomer sections could be clearly observed at Ug > 0.020 m s^{-1} in ALR. In fact, petroleum-based liquids are more resistant to the motion of gas bubbles and prevent the easy access to the liquid free surface. As a result, the gas-phase accumulation is observed at the top of downcomer for the ALR system. Moraveji et al. [28] demonstrated that the liquid circulation velocity in the riser-downcomer loop for diesel was much less than the pure water at ALRs under both laminar and turbulent regimes. It is noticed that, even at high inlet gas velocities, small vortexes formed at the top of the ALR. The streamlines in Fig. 6b show the recirculation of liquid phase through the downcomer region. A comparison of the flow pattern in Fig. 6a, and Fig. 6b indicates that the axial distribution of the liquid phase streamlines increases in ALR versus BCR. Fig. 6c shows that the vortexes described for ALR were decreased in ALR-NDT. One of the most important reasons for this phenomena is the presence of holes in the draft tube which led to the liquid or/and gas phases passing through them (some streamlines crossed through the net draft tube in Fig. 6c). It provides a further liquid circulation and improves the mixing behavior in terms of higher and unified gas volume fraction in the system. Besides, due to the netted structure of the draft tube in ALR-NDT, unlike in ALR, no mass aggregation of the gas-phase has been seen at the top of the downcomer region and the extensive distribution of the gas phase can be seen in ALR-NDT.

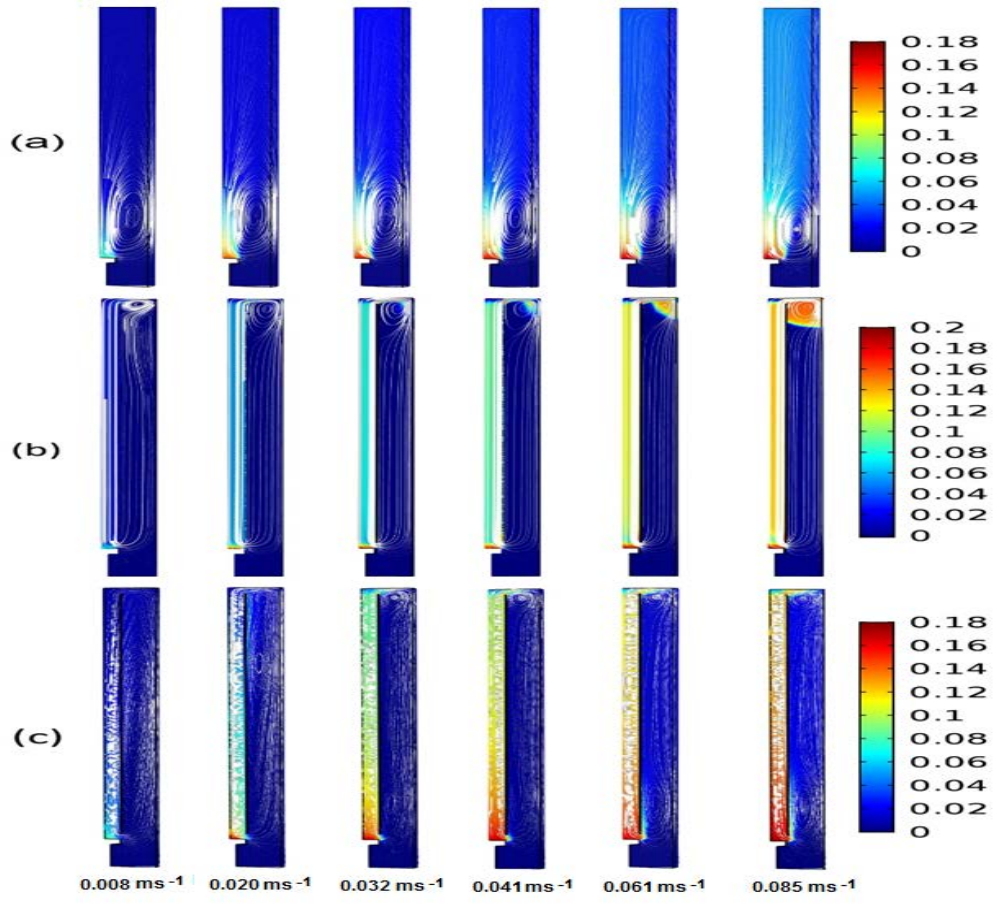

Figure 6. Snapshots of the gas concentration at a different gas velocity inlet at BCR (a), ALR (b), and ALR-NDT (c). White lines indicate the velocity streamlines of the liquid phase in the reactors.

Fig. 7a shows that the maximum liquid velocity is created above the gas diffuser in BCR and the maximum velocity magnitude is increased by increasing the inlet gas velocity. The high liquid velocity above the diffuser results in the formation of vortexes in the system which is presented at Fig. 6a. The liquid velocity showed a descending order with increasing altitude in the column of BCR and outside of the vortex zone, the magnitude of liquid velocity was lower than 0.05 m s^{-1}, even if the inlet gas velocity was increased to 0.085 m s^{-1}. Following the liquid velocity profile at Fig. 7b shows the liquid velocity in the riser of ALR was obviously increased by increasing the inlet gas velocity, while the downcomer liquid velocity was not affected by the inlet gas velocity. As expected, the liquid velocity at the riser region was higher than downcomer region in both ALR (Fig. 7b) and ALR-NDT (Fig. 7c) systems, however as shown at Fig. 7c, the net structure of the insert tube provides a possibility of the liquid passing through the net draft tube. It results in the velocity in the downcomer region being higher than ALR at the same inlet gas velocity.

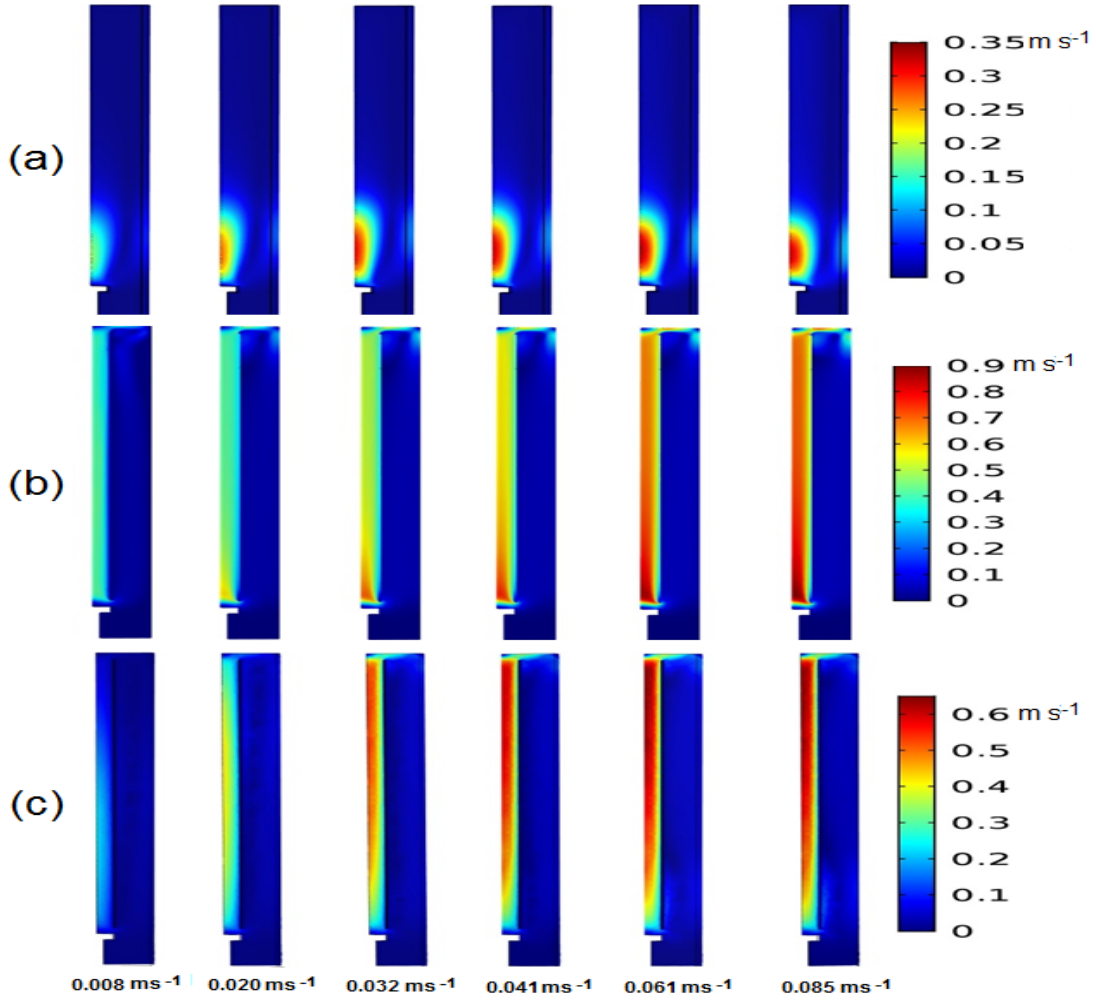

Figure 7. Snapshots of the liquid velocity magnitude at a different gas velocity inlet at BCR (a), ALR (b), and ALR-NDT (c).

3.4. Dead zones

Dead zones are usually designed into reactors for the removal of sediment at the bottom of reactors, however, they may have a negative

effect on the gas distribution and the mass transfer especially in biological processes [30]. Due to the elimination of mechanical mixing tools in BCR and ALR systems, the dead zone formation is a common phenomena in these reactors. Mahmood et al. [15] postulated the regions with the zero gas volume fraction as the dead zone. Loomba et al. [31] defined the dead zone as an area with a liquid velocity of less than 5 % of the volume average velocity magnitude. In this study, both the gas volume fraction and the mass transfer coefficient are considered to determine the dead zone in the test reactors. The results of Fig. 8 reveals that the dead zone has taken place at the bottom of all studied reactors. As shown in Fig. 8a-1, the dead zone mostly occurred at the bottom of the gas diffuser in BCR. The ALR had the broadest dead zone which especially formed at the bottom of the downcomer region (Fig. 8b-1). However, it can be seen at Fig. 8c-1 that ALR-NDT works with a minimum dead zone at about 8 % in comparison to two other geometries. Similar to the BCR, the dead zone corresponded to the bottom of the gas diffuser in ALR-NDT.

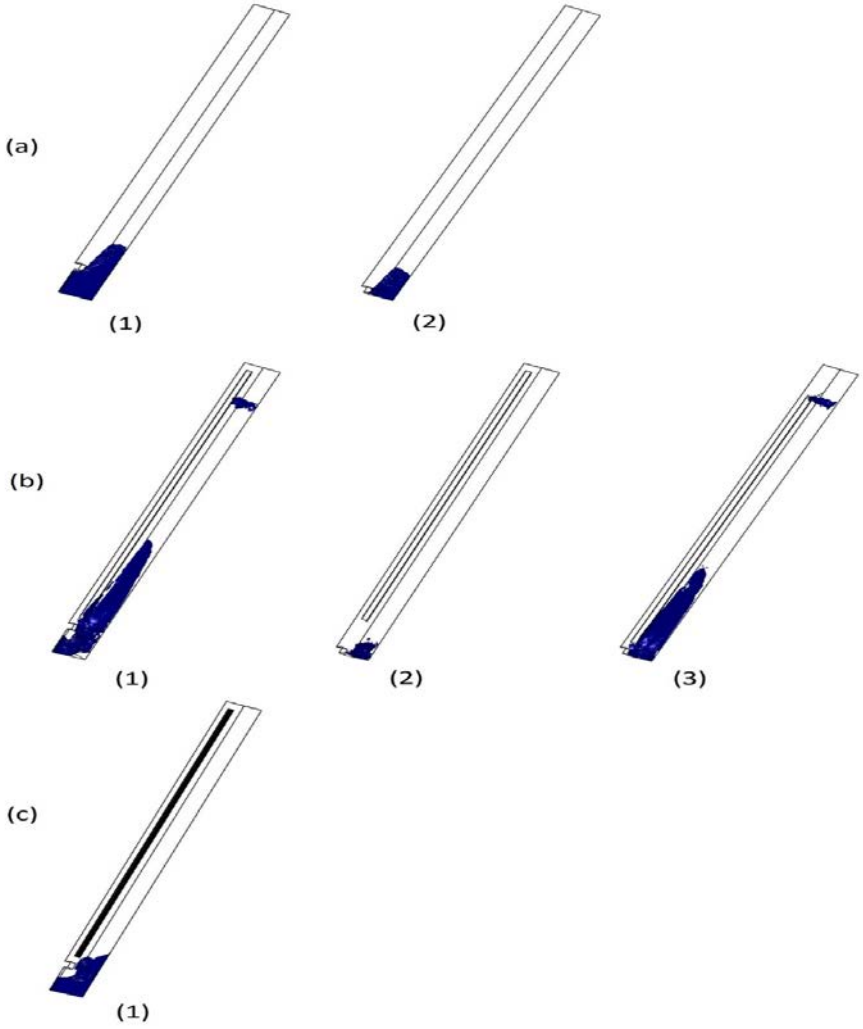

Figure 8. Areas with blue color indicating the regions with the zero mass transfer coefficient at the superficial gas velocity of 0.085 m s^{-1} in BCR (a), ALR (b), and ALR-NDT (c). 1: Original configuration, 2: Modified gas diffuser location, and 3: Simultaneous modification of the gas diffuser and draft tube locations.

In order to reduce the dead zone in BCR and ALR systems, the geometrical modifications of the components inside the reactors were evaluated. In BCR, only the location of the gas diffuser was examined when the gas inlet height to operational height was modified from 10:100 to 2:100 (Fig. 8a-2). While in the ALR system, two approaches were evaluated: Firstly, by keeping the draft tube at the previous position (the distance of draft tube from the bottom to the operational height was 12:100), the ratio of the gas diffuser height to the operational height was changed from 10:100 to 2:100 (Fig. 8b-2). Secondly, the height ratio of both the gas diffuser and the draft tube were simultaneously shifted from 10:100 to 2:100 (Fig. 8b-3). The results of geometrical modifications are also presented at Fig. 8. As it is seen at Fig. 8a-2, the dead zone has been decreased by 12 % with the modification of the gas diffuser location in BCR. At Fig. 8b-2, with the modification of the gas diffuser location and due to the increase of the distance between the gas diffuser and the draft tube, the dead zone was decreased by 40 % in ALR. Similar findings were reported by other researchers for ALR [15, 32]. However, when the draft tube and the gas diffuser simultaneously shifted to the bottom of the reactor, as seen at Fig. 8b-3, the circulation behavior was not improved in comparison with the original ALR geometry and thus the dead zone was not decreased.

4. Conclusions

In the present work, a 3D-CFD simulation by COMSOL Multiphysics based on a two-fluid Eulerian-Eulerian model described properly the experimental data of the gas holdup and the mass transfer coefficient in BCR, ALR, and ALR-NDT for the diesel-air system in both laminar and turbulent regimes. In agreement with previous experimental observations, the simulation showed that BCR had the maximum values of the holdup and the mass transfer coefficient in comparison to ALR and ALR-NDT, however some issues such as the vortex occurrence and the less liquid and the gas distribution in BCR make this reactor less efficient for hydrocarbon systems. On the other hand, the results of simulations revealed that the gas distribution in ALR-NDT specifically in the downcomer region was higher than the same in ALR. It was another reason that made it clear that ALR-NDT was more efficient than ALR in the mass transfer distribution. Moreover, the determination of the dead zones formation in the reactors is a crucial step in the successful scale up of the reactors. It is clarified by the simulation that the region lower than the position of the gas inlet was the most common region for the dead zone to take place. It was also determined the presence of NDT providing an optimal liquid circulation and a gas distribution, and thus ALR-NDT had the least amount of the dead zone among others.

Nomenclature

A	specific interfacial area [m^2 m^3].
C_d	viscous drag coefficient.
C_k	constant in k-ε model.
C_ε	model parameter in turbulent dissipation energy equation.
C_μ	constant in k-ε model.
d_b	bubble diameter [m].
D_L	molecular diffusivity of gas in liquid [m^2 s^{-1}].
Eö	Eötvös number.
F	volume force [N m^{-2}].
G	gravity constant [m s^{-2}].
h_f	aerated liquid height.
h_i	un-aerated liquid height.
k	turbulent kinetic energy per unit mass [m^2s^{-2}].
k_La	volumetric mass transfer coefficient [s^{-1}].
m_{gl}	mass transfer rate from gas to the liquid [kg m^{-3} s^{-1}].

P (p)	pressure [Pa].
Re_b	Reynolds number.
U (u)	velocity vector [m s^{-1}].
u_{slip}	relative velocity between gas and liquid.
V_f	volume of aerated liquid.
V_i	volume of un-aerated liquid.

Greek letters

ε	turbulent energy dissipation rate per unit mass [m^2 s^{-3}].
ε_g	gas holdup.
μ	viscosity [Pa.s].
ρ	density [kg m^{-3}].
σ	surface tension[N m^{-1}].
ϕ	phase volume fraction [m^3 m^{-3}].

References

[1] Kantarci, N., Borak, F. and Ulgen, K. O., "Bubble column reactors", *Process Biochem.*, **40** (7), 2263 (2005). (https://doi:10.1016/j.procbio.2004.10.004).

[2] Behin, J., "Modeling of modified airlift loop reactor with a concentric double-draft tube", *Chem. Eng. Res. Des.*, **88** (8), 919 (2010). (https://doi.org/10.1016/j.cherd.2010.01.004).

[3] Flickinger, M. C. and Drew, S. W., Encyclopedia of bioprocess technology, John Wiley, (1999).

[4] Fu, C. C., Wu, W. T. and Lu, S. Y., "Performance of airlift bioreactors with net draft tube", *Enzme. Microb. Technol.*, **33** (4), 332 (2003). (https://doi.org/10.1016/S0141-0229(03)00151-0).

[5] Mohebali, G. and Ball, A. S., "Biodesulfurization of diesel fuels-past, present and future perspectives", *Int. Biodeter. & Biodegrad.*, **110**, 163 (2016). (https://doi.org/10.1016/j.ibiod.2016.03.011).

[6] Tabib, M. V., Roy, S. A. and Joshi, J. B., "CFD simulation of bubble column-an analysis of interphase forces and turbulence models", *Chem. Eng. J.*, **139** (3), 589 (2008). (https://doi.org/10.1016/j.cej.2007.09.015).

[7] Azzopardi, B., Zhao, D, Yan, Y. and Zhao D., Hydrodynamics of gas-liquid reactors: Normal operation and upset conditions, John Wiley & Sons, (2011). (https://doi.org/10.1002/9781119970712).

[8] Lestinsky, P., Vayrynen, P., Vecer, M. and Wichterle, K., "Hydrodynamics of airlift reactor with internal circulation loop: Experiment vs. CFD simulation", *Procedia Eng.*, **42**, 892 (2012) (https://doi.org/10.1016/j.proeng.2012.07.482).

[9] Hekmat, A., Amooghin, A. E. and Moraveji, M. K., "CFD simulation of gas-liquid flow behaviour in an air-lift reactor: Determination of the optimum distance of the draft tube", *Simul. Model. Pract. Theory*, **18** (7), 927 (2010). (https://doi.org/10.1016/j.simpat.2010.02.009).

[10] Nalband, M. and Jalilnejad, E., "3D CFD simulation of gas hold-up and mass transfer in a modified airlift reactor with net draft tube", *Int. J. Chem. Reac. Eng.*, **17** (12), (2019). (https://doi.org/10.1515/ijcre-2019-0060).

[11] Lu, X., Long, B., Ding, Y. and Deng, F., "Experimental study and CFD-PBM simulation of the unsteady gas-liquid flow in an airlift external loop reactor", *Flow Turbul. Combust.*, **102** (4), 1053 (2019). (https://doi.org/10.1007/s10494-018-9992-5).

[12] Guler, B. A., Deniz, I., Demirel, Z. and Imamoglu, E., "Computational fluid dynamics simulation in scaling-up of airlift photobioreactor for astaxanthin production", *J. Biosci. Bioeng.*, **129** (1),

86 (2020). (https://doi.org/10.1016/j.jbiosc.2019.06.010).

[13] Dejaloud, A., Vahabzadeh, F. and Habibi, A., "Hydrodynamics and oxygen transfer characterization in a net draft tube airlift reactor with water-in-diesel microemulsion", *Fuel Processing Technology*, **171**, 265 (2018). (https://doi.org/10.1016/j.fuproc.2017.11.027).

[14] Kuzmin, D., Haario, H. and Turek S., "Finite element simulation of turbulent bubbly flows in gas-liquid reactors", Univ. Dortmund, Fachbereich Mathematik, Dortmund, Germany, (2005).

[15] Mahmood, K. A., Wilkinson, S. J. and Zimmerman, W. B., "Airlift bioreactor for biological applications with microbubble mediated transport processes", *Chem. Eng. Sci.*, **137**, 243 (2015). (https://doi.org/10.1016/j.ces.2015.06.032).

[16] Davarnejad, R., Bagheripoor, E. and Sahraei, A., "CFD simulation of scale influence on the hydrodynamics of an internal loop airlift reactor", S*ci. Res.*, **4** (10), 668 (2012). (https://doi.org/10.4236/eng.2012.410085).

[17] Salehpour, R., Jalilnejad, E., Nalband, M. and Ghasemzadeh, K., "Hydrodynamic behavior of an airlift reactor with net draft tube with different configurations: Numerical evaluation using CFD technique", *Particuology*, **51**, 91 (2019). (https://doi.org/10.1016/j.partic.2019.09.005).

[18] Crowe, C. T., Schwarzkopf, J. D., Sommerfeld, M. and Tsuji, Y., Multiphase flows with droplets and particles, CRC Press, (2011).

[19] Murthy, B. and Joshi J., "Assessment of standard k–ε, RSM and LES turbulence models in a baffled stirred vessel agitated by various impeller designs", *Chem. Eng. Sci.*, **63** (22), 5468 (2008). (http://doi.org/10.1016/j.ces.2008.06.019).

[20] Shaheed, R., Mohammadian A. and Gildeh, H. K., "A comparison of standard k–ε and realizable k–ε turbulence models in curved and confluent channels", *Environ. Fluid Mech.*, **19** (2), 543 (2019). (http://doi.org/ 10.1007/s10652-018-9637-1).

[21] Sokolichin, A. and Eigenberger, G., "Applicability of the standard k–ε turbulence model to the dynamic simulation of bubble columns: Part I. Detailed numerical simulations", *Chem. Eng. Sci.*, **54** (13-14), 2273 (1999). (https://doi.org/10.1016/S0009-2509(98)00420-5).

[22] Cockx, A., Do-Quang, Z., Line, A. and Roustan, M., "Use of computational fluid dynamics for simulating hydrodynamics and mass transfer in industrial ozonation towers", *Chem. Eng. Sci.*, **54** (21), 5085 (1999). (https://doi.org/10.1016/S0009-2509(99)00239-0).

[23] Moraveji, M. K., and Davarnejad, R., "CFD modeling of geometrical parameters effects on the hydrodynamics and mass transfer in an airlift reactor", *World Appl. Sci. J.*, **15** (6), 890 (2011).

[24] Chisti, Y., "Pneumatically agitated bioreactors in industrial and environmental bioprocessing: Hydrodynamics, hydraulics, and transport phenomena", *Appl. Mech. Rev.*, **51** (1), 33 (1998). (https://doi.org/10.1115/1.3098989).

[25] Suhaimi, A. and Nasir, N., "Study of the fluid flow pattern in a bubble column

reactor for biodiesel production", Proceedings of *IOP Conference Series: Materials Science and Engineering*, **1**, 012035 (2017).

[26] Moradi, S., Rajabi, Z., Mohammadi, M., Salimi, M., Homami, S. S., Seydei, M. K. and Shirazian, S., "3 dimensional hydrodynamic analysis of concentric draft tube airlift reactors with different tube diameters", *Math. Comput. Model.*, **57** (5-6), 1184 (2013). (https://doi.org/10.1016/j.mcm.2012.10.021).

[27] Wu, W. T. and Wu, J. Y., "Airlift reactor with net draught tube", *J. Ferm. Bioeng.*, **70** (5), 359 (1990). (https://doi.org/10.1016/0922-338X(90)90152-M).

[28] Moraveji, M. K., Mohsenzadeh, E., Fakhari, M. E. and Davarnejad, R., "Hydrodynamics and oxygen mass transfer characteristics of petroleum based micro-emulsions in a packed bed split-cylinder airlift reactor", *Braz. J. Chem. Eng.*, **30** (3), 541 (2013). (https://doi.org/10.1590/S0104-66322013000300012).

[29] Tunthikul, N., Wongsuchoto, P. and Pavasant, P., "Hydrodynamics and mass transfer behavior in multiple draft tube airlift contactors", *Korean J. Chem. Eng.*, **23** (6), 881 (2006). (https://doi.org/10.1007/s11814-006-0003-5).

[30] Jones, S. T. and Heindel, T. J., "Hydrodynamic considerations in an external loop airlift reactor with a modified downcomer", *Ind. Eng. Chem. Res.*, **49** (4), 1931 (2010). (https://doi.org/10.1021/ie901311r).

[31] Loomba, V., Huber, G. and von Lieres, E., "Single-cell computational analysis of light harvesting in a flat-panel photo-bioreactor", *Biotechnol. Biofuels*, **11** (1), 149 (2018). (https://doi.org/10.1186/s13068-018-1147-3).

[32] Amini, E., Mehrnia, M. R., Mousavi, S. M. and Azami, H., "Investigating the effect of sparger configuration on the hydrodynamics of a full-scale membrane bioreactor using computational fluid dynamics", *RSC Advances*, **5** (127), 105218 (2015). (https://doi.org/10.1039/C5RA18727C).